Original Article

The new fast kilovoltage-switching dual-energy computed tomography for measuring bone mineral density

Mingyue Wang^, Yan Wu, Yue Zhou, Junqiang Dong, Ping Hou, Jianbo Gao

Department of Radiology, The First Affiliated Hospital of Zhengzhou University, Zhengzhou, China

Contributions: (I) Conception and design: Y Wu, J Gao, J Dong; (II) Administrative support: J Gao, Yan Wu; (III) Provision of study materials or patients: P Hou, M Wang; (IV) Collection and assembly of data: Y Zhou, M Wang; (V) Data analysis and interpretation: J Dong, M Wang; (VI) Manuscript writing: All authors; (VII) Final approval of manuscript: All authors.

Correspondence to: Jianbo Gao. Department of Radiology, The First Affiliated Hospital of Zhengzhou University, No. 1 Jianshe East Road, Zhengzhou, China. Email: cjr.gaojianbo@vip.163.com.

Background: The update in technology may impact the accuracy in measuring bone mineral density (BMD). However, the application of the new fast kilovoltage (kV)-switching dual-energy computed tomography (DECT) for BMD measurement has not yet been reported. This study aimed to examine the accuracy and precision of the new fast kV-switching DECT in measuring BMD and to evaluate its applicability in clinical BMD measurement.

Methods: Forty sets of the new fast kV-switching DECT scans and one quantitative computed tomography (QCT) scan were performed on the European Spine Phantom. Their relative errors and relative standard deviations were compared. A retrospective analysis was performed on patients who underwent chest plain DECT and abdominal monoenergetic plain CT at the same time. The relationship between hydroxyapatite-water and hydroxyapatite-fat measured using DECT and BMD measured using QCT was analyzed by multivariate regression analysis.

Results: The relative errors of the new fast kV-switching DECT with low tube speeds (0.8 and 1.0 s/r) were all less than 6% and were less than those of QCT, except for those at 515 mA. The relative standard deviation values with high tube rotation speeds (0.5 and 0.6 s/r) were higher than those with low tube speeds (0.8 and 1.0 s/r) under most tube current conditions. The new fast kV-switching DECT-derived BMD values corrected by multiple linear regression (predicted hydroxyapatite) were significantly positively correlated with the QCT-based BMD values (R^2=0.912; P<0.001). The results of the Bland-Altman analysis demonstrated high consistency between the 2 measurement methods.

Conclusions: Results of the phantom measurements indicated that the new fast kV-switching DECT could measure BMD with relatively high accuracy and precision. The results of a subsequent clinical *in vivo* experiment demonstrated that vertebral BMD measurements derived from DECT and QCT were mostly consistent and highly accurate. Therefore, patients who undergo DECT for other clinical indications can simultaneously have their BMD determined.

Keywords: Bone density; dual-energy computed tomography (DECT); phantoms; accuracy; quantitative computed tomography (QCT)

Submitted Jul 01, 2022. Accepted for publication Nov 27, 2022. Published online Jan 05, 2023.
doi: 10.21037/qims-22-701
View this article at: https://dx.doi.org/10.21037/qims-22-701

^ ORCID: 0000-0003-0028-2231.

Introduction

Osteoporosis is characterized by decreased bone mass and deterioration of bone microstructure, which leads to increased bone fragility (1). Osteoporosis increases the incidence of bone fractures, which results in the poor quality of life for patients and a significant burden on their families (2,3). Over the past three decades, the prevalence of osteoporosis and the incidence of fragility fractures in China have increased considerably (4). In developed countries, the lifetime risk of fracture in people over 50 years old is about 50% in women and 20% in men (5). Bone mineral density (BMD) is an important index for the diagnosis and treatment of osteoporosis. Therefore, it is of great clinical and research significance to measure bone density accurately and conveniently.

Previous studies have explored the use of fast kilovoltage (kV)-switching dual-energy computed tomography (CT; FSDECT) to measure BMD (6-9). The new FSDECT technology has enabled ultrafast kV and milliamperage (mA) synchronized switching to achieve almost simultaneous dual-energy data acquisition. This update in technology may impact its accuracy in measuring BMD. However, the application of the new FSDECT for BMD measurement has not yet been reported. Therefore, this study aimed to investigate the accuracy and precision of the new FSDECT for measuring the BMD of the European Spine Phantom (ESP) and to evaluate the clinical applicability of the new FSDECT for BMD measurement.

Methods

Ex vivo phantom materials

The ESP (No. 145, QRM GmbH, Möhrendorf, Germany; *Figure 1A*) is mainly equivalent to hydroxyapatite (HAP) and water in X-ray attenuation, which comprises an epoxy resin and HAP (10). The 3 vertebral bodies of the ESP are named V1, V2, and V3 from top to bottom, and the corresponding HAP densities of cancellous bone are 51.0 mg/cm^3 (HAP50), 102.2 mg/cm^3 (HAP100), and 200.4 mg/cm^3 (HAP200), respectively (11). The exact HAP densities, as specified by the manufacturer, were used for all calculations and analyses; nominal values were only used for illustrative purposes in tables and figures.

Phantom scanning methods

Dual-energy CT (DECT) was performed using a 256-slice FSDECT scanner (Revolution Apex; GE Healthcare, Chicago, IL, USA). To explore the effect of different tube currents and rotation on the measurement of BMD, the scanning parameters were set as follows: fast tube voltage switching between high and low energy, 140/80 kVp; detector coverage, 80 mm; and pitch, 0.992:1. We established 40 sets of DECT scan parameters by separately combining tube rotation speeds of 0.5, 0.6, 0.8, and 1.0 s/r with 10 different tube currents (145, 200, 250, 300, 335, 370, 405, 445, 480, and 515 mA); 10 repeated scans were performed for each set of scan parameters.

Asynchronous calibration quantitative CT (QCT) was used in this study. The calibration phantom (Mindways Software Company, Inc., Austin, TX, USA) performed periodic calibration, and the phantom was not needed in the scanning process (*Figure 1B*). The parameters of QCT performed were as follows: tube voltage, 120 kVp; tube current, 140 mA; tube rotation speed, 0.6 s/r; pitch, 0.992:1; detector coverage, 80 mm; and scan field of view, 50 cm. The bed height was 145.5 cm, and calibration was performed using a fourth-generation calibration phantom. These scans were repeated 10 times. For the radiation dose, scan parameters for the various DECT groups and the volume CT dose index ($CTDI_{vol}$) values corresponding with the QCT scans were recorded.

Patient cohort for in vivo BMD measurements

The study was conducted in accordance with the Declaration of Helsinki (as revised in 2013). The study was approved by the ethics committee of Zhengzhou University, and individual consent for this retrospective analysis was waived. Patients who underwent conventional abdominal CT (including QCT, upper abdominal CT, or spinal CT) and DECT for thoracic scans between October 2021 and May 2022 were included. The interval between the abdominal and thoracic examinations did not exceed 1 month. *Figure 2* shows the flowchart of the study. *Table 1* shows the scan parameters of the participants.

Data measurement for the bone phantom and patients

The reconstructed DECT scan data were transferred to an Advantage Workstation 4.7 (GE Healthcare) for quantitative material measurement. The reconstructed abdominal data were transferred to a QCT Pro workstation (Mindways Software, Inc.) for QCT BMD measurement. Two attending physicians who did not know the scan

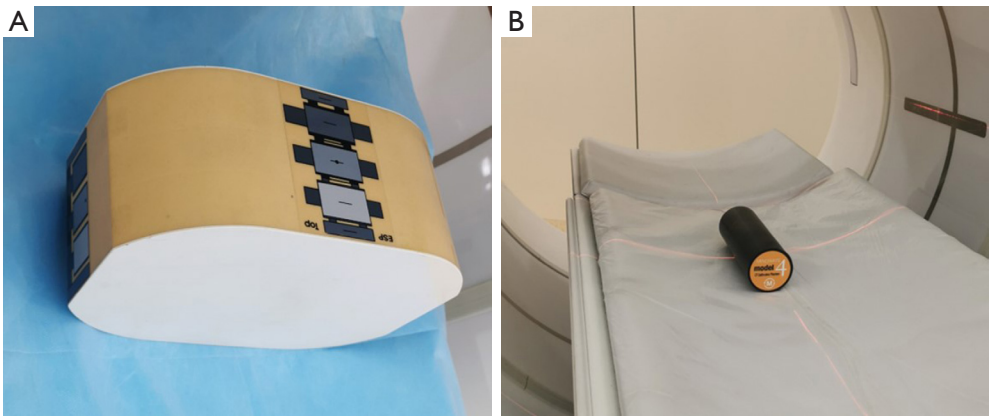

Figure 1 ESP and the calibration phantom used in QCT. (A) An anthropomorphic ESP. (B) Asynchronous phantom calibrated before the QCT scan. ESP, European Spine Phantom; QCT, quantitative computed tomography.

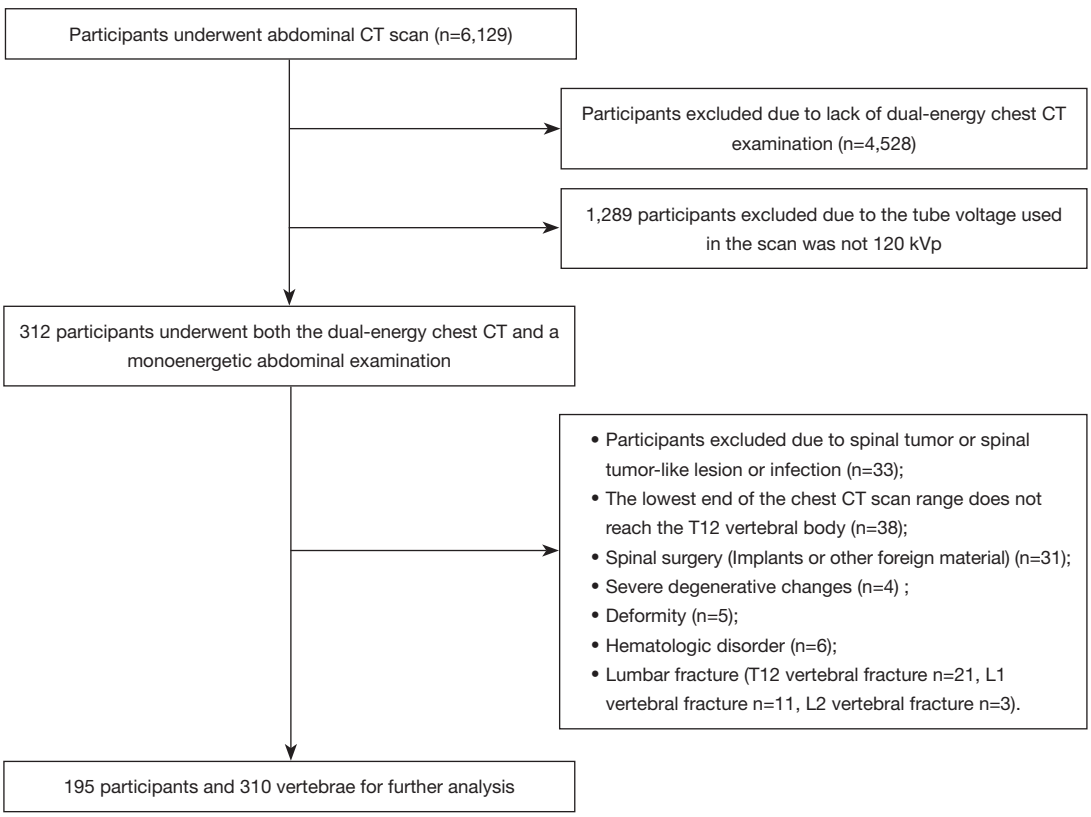

Figure 2 The flowchart of the patient screening process. CT, computed tomography.

methods separately conducted the measurements.

For the DECT measurement, during the measurement of the phantom, the circular region of interest (ROI) was set at the median plane of the vertebral body, with an area of 408.42 mm^2. As much cancellous bone as possible in the plane was included while areas with high BMD, such as the cortical bone and its pedicle, were avoided. For each patient, the ROI was two-thirds of the vertebral body size and was selected to avoid structures such as bone islands and the vertebral venous plexus. The HAP-water of the

Table 1 Scan parameters for dual-energy CT and abdominal CT

CT parameters	Scan mode	
	Abdominal CT	Dual-energy CT
Tube voltage (kVp)	120	80/140
Tube current (mA)	auto mA	GSI assist
Pitch	0.992:1	0.992:1
Tube speed (s/rot)	0.8	0.8
Slice thickness (mm)	1.25	1.25
ASIR-V	40%	40%

ASIR-V, adaptive statistical iterative reconstruction-Veo (data measurement for the bone phantom and patients); CT, computed tomography; GSI, gemstone spectral imaging.

phantom and the HAP-water and HAP-fat of the patients were measured.

For QCT measurements, the workstation software could generate and automatically analyze the ROIs. However, it needed to be reset if an obvious periprocedural error was observed.

Both phantom and patient data were measured twice at an interval of 1 week, and the average of the 2 measurements was used as the final value.

In order to compare the accuracy and precision of the ESP of SECT and QCT, we calculated the relative error (RE) and the relative standard deviation (RSD) using the method previously described (9). The formulas were as follows:

$$RE = \frac{BMD_{measured} - BMD_{ESP}}{BMD_{ESP}} \times 100\% \quad [1]$$

$$RSD = \frac{SD_{measured}}{n \times \sum BMD_{measured}} \times 100\% \quad [2]$$

where $BMD_{measured}$ is the measured BMD values of the ESP, BMD_{ESP} is the exact BMD values of the ESP, and $SD_{measured}$ is the standard deviation (SD) of the measured BMD values of the ESP.

Statistical analyses

Data were statistically analyzed using SPSS 25.0. (IBM Corp., Armonk, NY, USA). The 1-sample *t*-test was adopted to compare the differences between the measured HAP-water values of the V1, V2, and V3 vertebral bodies and true ESP values under different scan conditions.

BMD derived from DECT and QCT was analyzed using linear regression. The Bland-Altman analysis was used to assess the agreement between QCT-derived BMD and adjusted predicted BMD obtained from linear regression calibration. A 2-sided P value of 0.05 was used to indicate statistical significance.

Results

ESP results

Accuracy of ESP BMD measured by the new FSDECT

The DECT-based HAP-water values of V1, V2, and V3 of the ESP under different scan conditions are shown in *Table 2*. *Figure 3* shows the RE values of V1, V2, and V3 based on DECT under different scan conditions. The DECT-based measurement had positive and negative biases under different scan conditions. The RE absolute value range for DECT under various scan conditions was 0.10% (0.8 s/r; 145 mA) to 10.1% (0.6 s/r; 515 mA), 0.12% (0.6 s/r; 145 mA) to 6.9% (0.6 s/r; 515 mA) and 0.12% (0.8 s/r; 145 mA) to 6.1% (0.6 s/r; 515 mA) for V1, V2, and V3, respectively. For V1, V2, and V3, the absolute values of the RE of DECT under 0.8 s/r and 1.0 s/r were less than 6%, but there was an exception for V2 and V3 when the tube current was 515 mA.

Precision of ESP BMD measured by DECT

Figure 4 shows the RSD values for the various DECT conditions.

Results of the participants

In vivo DECT-based BMD measurements

Table 3 shows the characteristics of the participants. Based on the diagnostic criteria for osteoporosis in QCT, patients were divided into the osteoporosis group with BMD less than 80 mg/cm^3, the osteopenia group with BMD between 80 and 120 mg/cm^3, and the normal BMD group with BMD more than 120 mg/cm^3. Of the 310 vertebrae in our study, 55 had osteoporosis, 115 had osteopenia, and 140 had normal BMD. As shown in the scatter plots in *Figure 5*, HAP-water and HAP-fat exhibited linear relationships with QCT-based BMD; therefore, HAP-water and HAP-fatwere used to construct a multiple linear regression formula.

Table 2 Comparison of dual-energy computed tomography-based hydroxyapatite values using different scan protocols compared with the true values

Tube rotation speed (s/r)	Tube current (mA)	CTDIvol (mGy)	V1HAP (50 mg/cm^3)*	V2HAP (100 mg/cm^3)*	V3HAP (200 mg/cm^3)*
0.5	145	4.05	49.56±2.09†	98.02±1.60	193.36±4.42
0.5	200	5.12	52.07±1.58†	103.62±2.16†	199.64±2.31†
0.5	250	6.34	53.79±1.18	105.01±1.22	203.21±1.95
0.5	300	6.89	55.75±1.25	107.58±1.14	206.20±1.34
0.5	335	7.96	53.28±1.19	103.78±1.73	202.50±1.61
0.5	370	8.73	52.73±0.90	103.80±1.44	201.44±2.11†
0.5	405	9.93	51.46±0.92†	101.16±0.79	197.73±1.57
0.5	445	10.66	51.25±1.18†	101.01±1.13	197.45±1.21
0.5	480	11.61	50.53±0.78†	100.45±1.33	196.63±1.63
0.5	515	13.17	46.95±0.81	96.28±1.37	189.63±1.31
0.6	145	4.88	52.15±1.30	102.08±1.82†	198.37±1.91
0.6	200	6.27	55.04±1.03	106.51±1.34	205.85±1.89
0.6	250	7.81	55.89±0.74	107.87±0.88	208.50±1.19
0.6	300	8.62	51.68±1.13†	102.78±1.25†	202.71±1.75
0.6	335	9.92	55.60±1.90	107.26±1.94	207.37±2.69
0.6	370	10.87	51.91±1.02	103.14±1.00	200.34±1.25†
0.6	405	12.3	50.77±0.65†	101.47±1.28†	199.12±1.63
0.6	445	13.26	48.42±0.90	98.45±1.12	194.74±1.35
0.6	480	14.39	49.57±0.55	99.53±1.11	196.22±1.82
0.6	515	16.15	45.84±0.97	95.14±1.01	188.17±1.63
0.8	145	6.56	51.05±1.35	102.67±0.57	200.63±1.69†
0.8	200	8.6	56.54±0.72	108.91±0.98	208.11±1.63
0.8	250	10.7	53.59±0.68	105.27±1.18	205.53±1.12
0.8	300	12.11	51.63±0.64	103.37±0.85	202.93±1.49
0.8	335	13.81	51.24±0.73†	102.99±1.20†	201.97±1.27
0.8	370	15.17	51.27±1.03†	103.10±0.72	201.14±0.94
0.8	405	17.02	50.34±0.69	100.98±1.00	198.49±1.07
0.8	445	18.41	50.67±0.58†	101.08±0.76	198.75±0.75
0.8	480	19.97	50.23±0.80	100.79±0.68	198.42±0.78
0.8	515	22.17	47.24±0.43	96.99±0.84	193.01±0.97
1.0	145	8.2	51.30±0.89†	101.99±1.27†	202.05±1.90
1.0	200	10.92	54.10±1.13	105.30±0.88	206.41±1.09
1.0	250	13.57	52.86±0.71	103.29±1.21	204.50±1.13
1.0	300	15.56	52.51±0.82	102.74±0.83†	203.67±0.97
1.0	335	17.69	51.26±0.55†	101.47±1.00	200.56±1.05†
1.0	370	19.45	50.50±0.67	101.14±0.94	198.81±1.41
1.0	405	21.73	52.62±0.98	103.54±0.99	202.76±1.44
1.0	445	23.55	51.28±0.57†	101.59±0.88†	200.38±1.07†
1.0	480	25.51	49.16±0.60	99.29±0.92	197.10±1.02
1.0	515	28.15	48.08±0.35	98.32±0.98	194.75±1.25

The values are presented as mean ± standard deviation. *, phantom-specific concentrations (ESP-145; 51, 102.2, and 200.4 mg/cm^3 HAP were used to determine measurement error); †, the difference was insignificant compared with the true value. BMD, bone mineral density; CTDIvol, computed tomography dose index; DECT, dual-energy computed tomography; HAP, hydroxyapatite; QCT, quantitative computed tomography; ESP-145, European Spine Phantom-145.

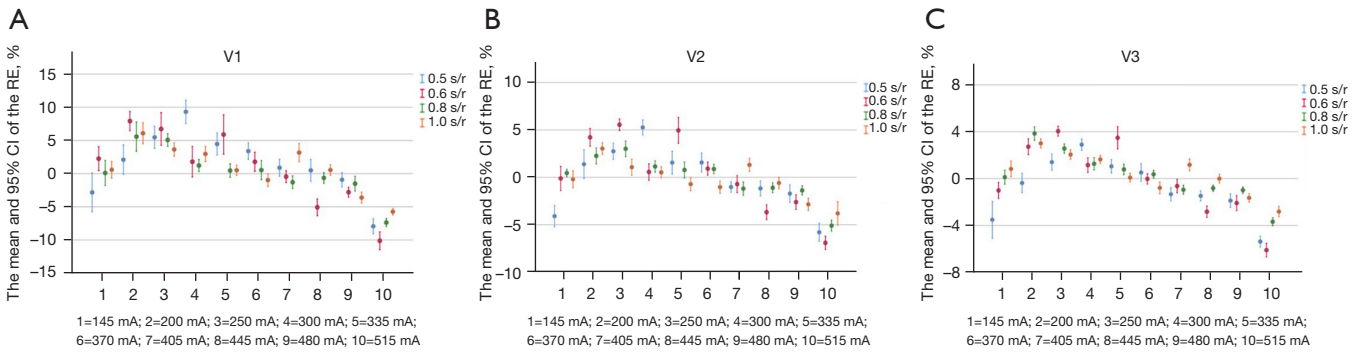

Figure 3 RE values under different scan conditions. RE values of (A) V1, (B) V2, and (C) V3 obtained under different scan conditions. The graphs show the plot of RE between the DECT-based HAP values and the true ESP values. Different colors represent different tube rotation speeds. The circle in the middle of each bar represents the mean RE value, and the upper and lower bounds represent the 95% confidence intervals. ESP, European Spine Phantom; HAP, hydroxyapatite; QCT, quantitative computed tomography; RE, relative error; DECT, dual-energy computed tomography; CI, confidence interval.

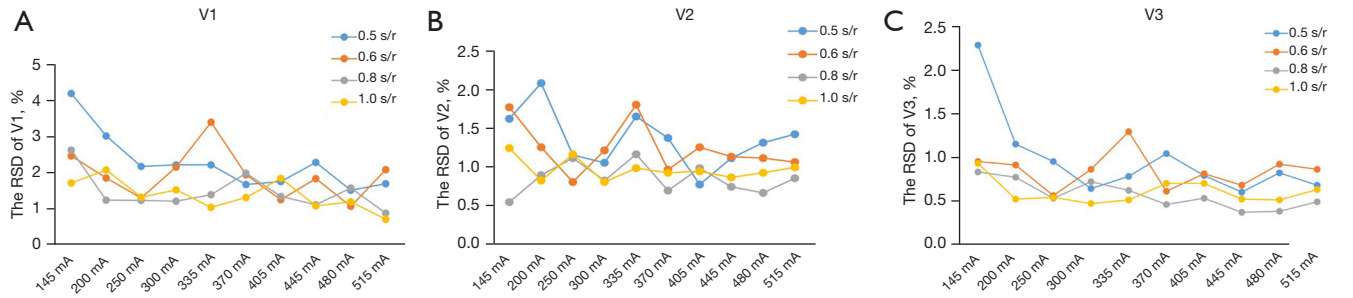

Figure 4 RSD values under different scan conditions. RSD values of (A) V1, (B) V2, and (C) V3 obtained under different scan conditions. RSD, relative standard deviation.

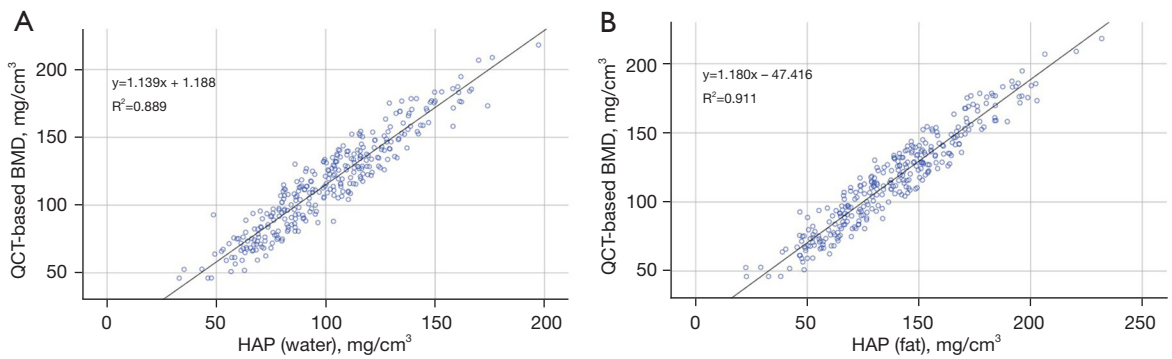

Figure 5 The comparison between QCT-based BMD values and HAP. Scatter plots showing the BMD values of 310 vertebral bodies of 195 patients. (A) QCT-based BMD values exhibited linear relationships with HAP (water). (B) The same trend was observed with HAP (fat). BMD, bone mineral density; HAP, hydroxyapatite; QCT, quantitative computed tomography.

The 3 groups were used for stratified sampling, resulting in 70% of the vertebrae (n=217) being used as the training set for regression modeling and 30% of the vertebrae (n=93) being used as the validation set to validate the regression model.

Results showed that the effects of HAP-water (b=–0.754; t=–3.4713; P=0.001) and HAP-fat (b=1.941; t=8.793; P<0.001) on QCT-based BMD were significant, with a constructed regression formula as follows:

$$\hat{y} = -0.75x_1 + 1.94x_2 - 72.23 \quad [3]$$

where $\hat{y}$ is the predicted value calculated from DECT-based HAP-water and HAP-fat, x_1 is HAP-water, and x_2 is HAP-fat.

The DECT-based BMD values calculated using multiple linear regression from the validation set (n=93) were significantly positively correlated with the QCT-based BMD values (R^2 =0.912; P<0.001). The mean difference between the 2 methods was –1.01 (P=0.344), and the majority of differences lay within ±1.96 SD without exhibiting an obvious trend. This demonstrates high consistency between the 2 measurement methods (*Figure 6*).

Table 3 Characteristics of the participants

Characteristics	T12	L1	L2
Age (years)	55.87±11.74	57.26±11.92	54.19±12.67
Gender			
Male	78 (42.6%)	44 (41.5%)	8 (38%)
Female	105 (57.4%)	62 (58.5%)	13 (62%)

The values for age are presented as mean ± standard deviation; the values for sex are presented as a number (%).

Discussion

In this study, we observed that the new FSDECT measurements under different scan conditions were not identical. Both positive and negative REs were obtained for the 3 ESP vertebral bodies, with RE ranges of –10.1% to 9.3%, –6.9% to 5.5%, and –6.1% to 4.0% for V1, V2, and V3, respectively. These ranges were all within the acceptable limits of clinical practice for osteoporosis screening (12,13). An error of several milligrams per cubic centimeter is not significant in the screening of osteoporosis, considering that there is at least a 40 mg/cm^3 difference in BMD between normal individuals (more than 120 mg/cm^3) and those with osteoporosis (less than 80 mg/cm^3) (14). The QCT results showed positive biases, which were consistent with the previous study (11). The systematic error for QCT volumetric BMD measurements means that follow-up scans on individual cases should be performed on the same CT system.

In another ESP-based study by Huang *et al.* (8), the largest REs for V1, V2, and V3 were 39.74%, 24.48%, and 20.56%, respectively. The differences in results might

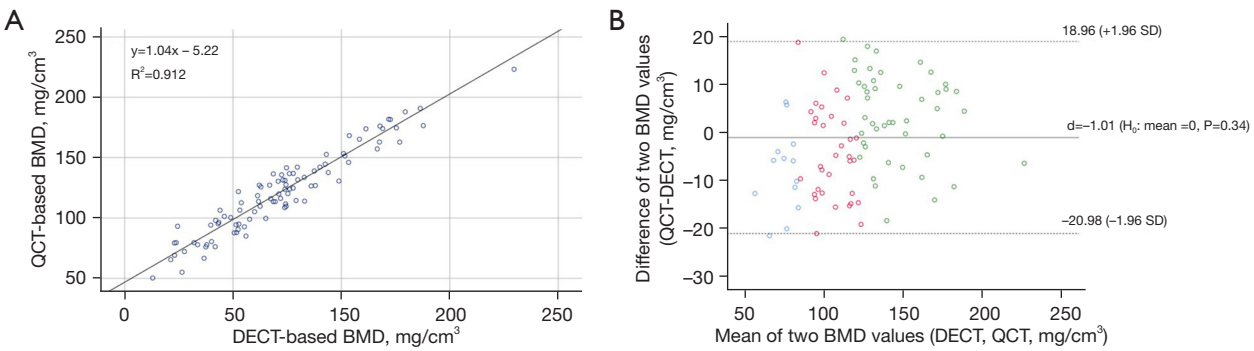

Figure 6 The consistency between DECT-based and QCT-based BMD values. (A) DECT-based BMD values calculated using multiple linear regression from the validation set (n=93) positively correlated with the QCT-based BMD values (R^2 =0.912; P<0.001). (B) The Bland-Altman plot of BMD assessment of 93 vertebral bodies. The x-axis represents the average BMD value obtained by DECT and QCT; the y-axis represents the difference between the 2 measurement methods (QCT-DECT). The solid line indicates the d between the 2 methods, and the dotted lines denote the 95% limits of agreement (d ± 1.96 SD). Given d =–1.01 (P=0.34) and SD =10.19 mg/cm^3, the ± 1.96 SD were 18.96 mg/cm^3 and –20.98 mg/cm^3, respectively. Different colored circles represent different BMD groups. The results show that the 2 measurement methods are highly consistent. d: mean difference; BMD, bone mineral density; CI, confidence interval; DsDECT, double-switching dual-energy computed tomography; QCT, quantitative computed tomography; SD, standard deviation.

have occurred because traditional switching DECT was employed by Huang *et al.* (8), whereas the new FSDECT was used in the present study. Technical advances have helped achieve improved quantification accuracy with the newer FSDECT scanner; these advances include more powerful tubes, more advanced detectors, and superior X-ray spectral properties (15).

In the present study, the absolute RE obtained with 27 sets of scan conditions was less than 1%, which is comparable to the results obtained by Koch *et al.* (16) in a phantom study conducted using dual-source DECT. Our RE values were also lower than those reported by Li *et al.* (17) in another phantom study using DECT. Van Hamersvelt *et al.* (13) and Mei *et al.* (18) found that RE increased with a decrease in tube current and deduced that a reduction in tube current caused a decrease in the number of emitted photons, thereby causing a decrease in the number of photons hitting the detector. This phenomenon may affect the accuracy of mass attenuation coefficients, thereby affecting the accuracy of BMD quantification. However, the measurement error did not correlate with the tube current in this study. Therefore, the specific roles of tube current warrant further investigation.

An important finding of the study is that the REs of the 3 vertebral ESP bodies were not reduced under low tube current conditions as compared with REs produced at high tube currents; hence, lower dose settings can be used in the new FSDECT to determine BMD. When a tube rotation speed of 0.8 s/r and a tube current of 145 mA were adopted, the REs of V1, V2, and V3 were –0.83%, 0.58%, and 0.16%, respectively. This finding may be related to the fact that the update of the X-ray tube improved the effective flux utilization per unit of time. By rapidly changing kV and mA via digital cathodes, the output flux of the tube was rapidly increased to match the power of the high-energy field of view without compromising the large-angle sampling speed and spatial resolution performance, resulting in higher accuracy at a low tube current.

When the precision of DECT was assessed, we found that the changes in relative SD (RSD) among different tube currents were greater at tube rotation speeds of 0.5 and 0.6 s/r. Additionally, the RSD values at these tube rotation speeds were higher than those at 0.8 and 1.0 s/r under most tube current conditions. A possible cause of this finding was inadequate energy spectral data acquisition at excessively high tube rotation speeds. Therefore, tube rotation speeds of 0.8 or 1.0 s/r are recommended when measuring BMD using DECT.

This study compared 2 direct methods (DECT and QCT) for the *in vivo* measurement of BMD in clinical participants. Vertebral bodies mainly comprise bone minerals—with HAP being a representative material chemically similar to the human bone—water, medulla ossium rubra, and medulla ossium flava, which mostly contain fat. Therefore, we assessed the contents of HAP-water and HAP-fat. During the QCT process, asynchronous QCT calibration was performed, which eliminated the need for a BMD calibration phantom. However, while researchers have recommended the use of DECT for the quantification of BMD, previous studies comparing BMD measurements obtained using DECT and dual-energy X-ray absorptiometry (DXA) have reported widely differing results.

Dong *et al.* (19) and Wichmann *et al.* (7) compared the performances of DECT and DXA for measuring BMD and concluded that DECT could be used to assess lumbar spine BMD. Another study reported that DECT showed more sensitivity to changes in BMD than did DXA and that the measurements of BMD using DECT and DXA were highly correlated (20). Conversely, Wesarg *et al.* (6) reported that DECT-derived BMD measurements had no correlation or were only moderately linearly correlated with DXA-derived BMD measurements. The differences among the studies described above may be related to the fact that DXA measures the area BMD and cannot distinguish cancellous bone from cortical bone. Roski *et al.* (21) compared BMD measurements derived from DECT and QCT and suggested that DECT-based quantification of BMD is feasible and may be applied in clinical practice; however, as the study was performed using dual-layer spectral CT, the results were not applicable to fast-switching DECT.

Feasibility studies of *in vivo*, phantomless BMD assessments were separately performed by Booz *et al.* (22), who used dual-source DECT, and Liu *et al.* (23), who used FSDECT. Michalski *et al.* (24) and Bartenschlager *et al.* (25) have demonstrated the accuracy of phantomless BMD measurement. However, further research is needed due to the impact of improved technology on the accuracy of BMD measurements. In the present study, we performed a clinical, *in vivo* study of 310 vertebral bodies of 195 participants after validating the accuracy of the new FSDECT measurements using a bone phantom. Multiple linear regression analysis was conducted with HAP-water, HAP-fat, and QCT-based BMD measurements. The results

indicated that the adjusted predicted HAP values, obtained after correction by multiple linear regression, significantly positively correlated with the QCT-based BMD values. The Bland-Altman plot also revealed that the 2 methods of measurement were highly consistent, which demonstrated the capability of the new FSDECT to accurately measure the BMD of vertebral bodies *in vivo*.

Previous research has shown that DECT is superior to conventional CT in differentiating between benign and malignant tumors and detecting disease, and DECT has been widely used in thoracic and abdominal scanning (26-29). DECT has other advantages, such as improving image quality and eliminating metal artifacts (30,31). Therefore, simultaneous osteoporosis screening can be performed during thoracic and abdominal CT to eliminate the need for additional radiation doses.

The present study has certain limitations. The design was retrospective, and the thoracic CT scan range differed among participants. Consequently, only a small number of L2 vertebral bodies were included in our analysis. The International Society for Clinical Densitometry recommends the use of mean L1–L2 values for diagnosis with QCT (32); the alternative use of the T12 and L3 values is only recommended when assessment conditions are not satisfied by L1 and L2. Therefore, a larger number of L2 vertebral bodies should be included in assessment in future studies.

Conclusions

In conclusion, results of the phantom measurements indicate that the new FSDECT could achieve relatively high accuracy and precision for BMD measurement. The results of a subsequent clinical *in vivo* experiment demonstrated that vertebral BMD measurements derived from DECT and QCT were mostly consistent and highly accurate. Therefore, patients who undergo DECT for other clinical indications, such as oncology staging and workup in emergency presentations, can have their BMD determined simultaneously.

Acknowledgments

We would like to thank Dr. Luotong Wang and Dr. Xuan Zhang from GE Healthcare, China, for technical CT guidance.

Funding: This study was supported by the Scientific Research Project plan of Henan Province (No. HNGD2022033).

Footnote

Conflicts of Interest: All authors have completed the ICMJE uniform disclosure form (available at https://qims.amegroups.com/article/view/10.21037/qims-22-701/coif). The authors have no conflicts of interest to declare.

Ethical Statement: The authors are accountable for all aspects of the work in ensuring that questions related to the accuracy or integrity of any part of the work are appropriately investigated and resolved. The study was conducted in accordance with the Declaration of Helsinki (as revised in 2013). The study was approved by the ethics committee of Zhengzhou University, and individual consent for this retrospective analysis was waived.

References

1. Zeng Q, Li N, Wang Q, Feng J, Sun D, Zhang Q, Huang J, Wen Q, Hu R, Wang L, Ma Y, Fu X, Dong S, Cheng X. The Prevalence of Osteoporosis in China, a Nationwide, Multicenter DXA Survey. J Bone Miner Res 2019;34:1789-97.
2. Levin VA, Jiang X, Kagan R. Estrogen therapy for osteoporosis in the modern era. Osteoporos Int 2018;29:1049-55.
3. Zhou S, Zhu L, You T, Li P, Shen H, He Y, Gao H, Yan L, He Z, Guo Y, Zhang Y, Zhang K. In vivo quantification of bone mineral density of lumbar vertebrae using fast kVp switching dual-energy CT: correlation with quantitative computed tomography. Quant Imaging Med Surg 2021;11:341-50.
4. Chen P, Li Z, Hu Y. Prevalence of osteoporosis in China: a meta-analysis and systematic review. BMC Public Health 2016;16:1039.
5. Sànchez-Riera L, Carnahan E, Vos T, Veerman L,

Norman R, Lim SS, Hoy D, Smith E, Wilson N, Nolla JM, Chen JS, Macara M, Kamalaraj N, Li Y, Kok C, Santos-Hernández C, March L. The global burden attributable to low bone mineral density. Ann Rheum Dis 2014;73:1635-45.
6. Wesarg S, Kirschner M, Becker M, Erdt M, Kafchitsas K, Khan MF. Dual-energy CT-based assessment of the trabecular bone in vertebrae. Methods Inf Med 2012;51:398-405.
7. Wichmann JL, Booz C, Wesarg S, Kafchitsas K, Bauer RW, Kerl JM, Lehnert T, Vogl TJ, Khan MF. Dual-energy CT-based phantomless in vivo three-dimensional bone mineral density assessment of the lumbar spine. Radiology 2014;271:778-84.
8. Huang S, Cui X, Han H, Zhang Y, Gao B, Yu W. Study on the scanning protocols for measuring bone mineral density by gemstone CT spectral imaging based on European spine phantom. Acta Radiol 2021. [Epub ahead of print]. doi: 10.1177/02841851211063014.
9. Booz C, Noeske J, Albrecht MH, Lenga L, Martin SS, Yel I, Huizinga NA, Vogl TJ, Wichmann JL. Diagnostic accuracy of quantitative dual-energy CT-based bone mineral density assessment in comparison to Hounsfield unit measurements using dual x-ray absorptiometry as standard of reference. Eur J Radiol 2020;132:109321.
10. Pearson J, Dequeker J, Henley M, Bright J, Reeve J, Kalender W, Laval-Jeantet AM, Rüegsegger P, Felsenberg D, Adams J. European semi-anthropomorphic spine phantom for the calibration of bone densitometers: assessment of precision, stability and accuracy. The European Quantitation of Osteoporosis Study Group. Osteoporos Int 1995;5:174-84.
11. Zhao Y, Li K, Duanmu Y, Wang L, Xu X, Zhang Y, Tang J, Zhang Y, Li Z, Hind K, Blake GM, Cheng X. Accuracy, Linearity and Precision of Spine QCT vBMD Phantom Measurements for Different Brands of CT Scanner: A Multicentre Study. J Clin Densitom 2022;25:34-42.
12. Wu Y, Jiang Y, Han X, Wang M, Gao J. Application of low-tube current with iterative model reconstruction on Philips Brilliance iCT Elite FHD in the accuracy of spinal QCT using a European spine phantom. Quant Imaging Med Surg 2018;8:32-8.
13. Van Hamersvelt RW, Schilham AMR, Engelke K, den Harder AM, de Keizer B, Verhaar HJ, Leiner T, de Jong PA, Willemink MJ. Accuracy of bone mineral density quantification using dual-layer spectral detector CT: a phantom study. Eur Radiol 2017;27:4351-9.
14. Brown JK, Timm W, Bodeen G, Chason A, Perry M, Vernacchia F, DeJournett R. Asynchronously Calibrated Quantitative Bone Densitometry. J Clin Densitom 2017;20:216-25.
15. Sugawara H, Takayanagi T, Ishikawa T, Katada Y, Fukui R, Yamamoto Y, Suzuki S. New Fast kVp Switching Dual-Energy CT: Reduced Severity of Beam Hardening Artifacts and Improved Image Quality in Reduced-Iodine Virtual Monochromatic Imaging. Acad Radiol 2020;27:1586-93.
16. Koch V, Hokamp NG, Albrecht MH, Gruenewald LD, Yel I, Borggrefe J, et al. Accuracy and precision of volumetric bone mineral density assessment using dual-source dual-energy versus quantitative CT: a phantom study. Eur Radiol Exp 2021;5:43.
17. Li X, Li X, Li J, Jiao X, Jia X, Zhang X, Fan G, Yang J, Guo J. The accuracy of bone mineral density measurement using dual-energy spectral CT and quantitative CT: a comparative phantom study. Clin Radiol 2020;75:320.e9-320.e15.
18. Mei K, Schwaiger BJ, Kopp FK, Ehn S, Gersing AS, Kirschke JS, Muenzel D, Fingerle AA, Rummeny EJ, Pfeiffer F, Baum T, Noël PB. Bone mineral density measurements in vertebral specimens and phantoms using dual-layer spectral computed tomography. Sci Rep 2017;7:17519.
19. Yue D, Li Fei S, Jing C, Ru Xin W, Rui Tong D, Ai Lian L, Luo YH. The relationship between calcium (water) density and age distribution in adult women with spectral CT: initial result compared to bone mineral density by dual-energy X-ray absorptiometry. Acta Radiol 2019;60:762-8.
20. Wait JM, Cody D, Jones AK, Rong J, Baladandayuthapani V, Kappadath SC. Performance Evaluation of Material Decomposition With Rapid-Kilovoltage-Switching Dual-Energy CT and Implications for Assessing Bone Mineral Density. AJR Am J Roentgenol 2015;204:1234-41.
21. Roski F, Hammel J, Mei K, Baum T, Kirschke JS, Laugerette A, Kopp FK, Bodden J, Pfeiffer D, Pfeiffer F, Rummeny EJ, Noël PB, Gersing AS, Schwaiger BJ. Bone mineral density measurements derived from dual-layer spectral CT enable opportunistic screening for osteoporosis. Eur Radiol 2019;29:6355-63.
22. Booz C, Hofmann PC, Sedlmair M, Flohr TG, Schmidt B, D'Angelo T, Martin SS, Lenga L, Leithner D, Vogl TJ, Wichmann JL. Evaluation of bone mineral density of the lumbar spine using a novel phantomless dual-energy CT post-processing algorithm in comparison with dual-energy X-ray absorptiometry. Eur Radiol Exp 2017;1:11.
23. Liu ZJ, Zhang C, Ma C, Qi H, Yang ZH, Wu HY, Yang

KD, Lin JY, Wong TM, Li ZY, Li CH, Ding Y. Automatic phantom-less QCT system with high precision of BMD measurement for osteoporosis screening: Technique optimisation and clinical validation. J Orthop Translat 2022;33:24-30.
24. Michalski AS, Besler BA, Michalak GJ, Boyd SK. CT-based internal density calibration for opportunistic skeletal assessment using abdominal CT scans. Med Eng Phys 2020;78:55-63.
25. Bartenschlager S, Dankerl P, Chaudry O, Uder M, Engelke K. BMD accuracy errors specific to phantomless calibration of CT scans of the lumbar spine. Bone 2022;157:116304.
26. Li M, Zhang L, Tang W, Ma PQ, Zhou LN, Jin YJ, Qi LL, Wu N. Quantitative features of dual-energy spectral computed tomography for solid lung adenocarcinoma with EGFR and KRAS mutations, and ALK rearrangement: a preliminary study. Transl Lung Cancer Res 2019;8:401-12.
27. Fehrmann A, Garcia Borrega J, Holz J, Shapira N, Doerner J, Boell B, Maintz D, Hickethier T. Metastatic pulmonary calcification: First report of pulmonary calcium suppression using dual-energy CT. Radiol Case Rep 2020;15:900-3.
28. Wang X, Liu D, Zeng X, Jiang S, Li L, Yu T, Zhang J. Dual-energy CT quantitative parameters for the differentiation of benign from malignant lesions and the prediction of histopathological and molecular subtypes in breast cancer. Quant Imaging Med Surg 2021;11:1946-57.
29. Nagayama Y, Tanoue S, Inoue T, Oda S, Nakaura T, Utsunomiya D, Yamashita Y. Dual-layer spectral CT improves image quality of multiphasic pancreas CT in patients with pancreatic ductal adenocarcinoma. Eur Radiol 2020;30:394-403.
30. Kang HJ, Lee JM, Lee SM, Yang HK, Kim RH, Nam JG, Karnawat A, Han JK. Value of virtual monochromatic spectral image of dual-layer spectral detector CT with noise reduction algorithm for image quality improvement in obese simulated body phantom. BMC Med Imaging 2019;19:76.
31. Tahmasebi Birgani MJ, Mahdavi M, Zabihzadeh M, Lotfi M, Mosleh-Shirazi MA. Simultaneous characterization of electron density and effective atomic number for radiotherapy planning using stoichiometric calibration method and dual energy algorithms. Australas Phys Eng Sci Med 2018;41:601-19.
32. Shepherd JA, Schousboe JT, Broy SB, Engelke K, Leslie WD. Executive Summary of the 2015 ISCD Position Development Conference on Advanced Measures From DXA and QCT: Fracture Prediction Beyond BMD. J Clin Densitom 2015;18:274-86.

Cite this article as: Wang M, Wu Y, Zhou Y, Dong J, Hou P, Gao J. The new fast kilovoltage-switching dual-energy computed tomography for measuring bone mineral density. Quant Imaging Med Surg 2023;13(2):801-811. doi: 10.21037/qims-22-701

